

A SEARCH FOR THE HIGGS BOSON PRODUCED IN ASSOCIATION WITH TOP QUARKS IN MULTILEPTON FINAL STATES AT ATLAS

Chris Lester

A DISSERTATION
in
Physics and Astronomy

Presented to the Faculties of The University of Pennsylvania
in Partial Fulfillment of the Requirements for the Degree of Doctor of Philosophy
2014

Joseph Kroll, Professor, Physics
Supervisor of Dissertation

A.T. Charlie Johnson, Professor, Physics
Graduate Group Chairperson

Dissertation Committee

Randall Kamien, Professor, Physics

I. Joseph Kroll, Professor, Physics

Elliot Lipeles, Assistant Professor, Physics

Burt Ovrut, Professor, Physics

Joseph Kroll, Professor, Physics

A SEARCH FOR THE HIGGS BOSON PRODUCED IN ASSOCIATION WITH TOP QUARKS IN MULTILEPTON FINAL STATES AT ATLAS

COPYRIGHT
2014
Chris Lester

All rights reserved.

Acknowledgements

30 Acknowledgements acknowledgements acknowledgements acknowledgements acknowledgements ac-
31 knowledgements acknowledgements acknowledgements acknowledgements acknowledgements acknowl-
32 edgements acknowledgements acknowledgements acknowledgements acknowledgements acknowledgements
33 acknowledgements acknowledgements acknowledgements acknowledgements acknowledgements acknowledgements
34 acknowledgements acknowledgements acknowledgements acknowledgements acknowledgements acknowledgements
35 acknowledgements acknowledgements.

36 Acknowledgements acknowledgements acknowledgements acknowledgements acknowledgements ac-
37 knowledgements acknowledgements acknowledgements acknowledgements acknowledgements acknowledgements
38 acknowledgements acknowledgements acknowledgements acknowledgements acknowledgements acknowledgements
39 acknowledgements acknowledgements acknowledgements acknowledgements acknowledgements acknowledgements
40 acknowledgements acknowledgements acknowledgements acknowledgements acknowledgements acknowledgements
41 acknowledgements acknowledgements.

42 Acknowledgements acknowledgements acknowledgements acknowledgements acknowledgements ac-
43 knowledgements acknowledgements acknowledgements acknowledgements acknowledgements acknowledgements
44 acknowledgements acknowledgements acknowledgements acknowledgements acknowledgements acknowledgements
45 acknowledgements acknowledgements acknowledgements acknowledgements acknowledgements acknowledgements
46 acknowledgements acknowledgements acknowledgements acknowledgements acknowledgements acknowledgements
47 acknowledgements acknowledgements.

48

ABSTRACT

49

A SEARCH FOR THE HIGGS BOSON PRODUCED IN ASSOCIATION WITH TOP
50 QUARKS IN MULTILEPTON FINAL STATES AT ATLAS

51

Chris Lester

52

Joseph Kroll

53

Abstract abstract abstract abstract abstract abstract abstract abstract abstract
54 abstract abstract abstract abstract abstract abstract abstract abstract abstract
55 abstract abstract abstract abstract abstract abstract abstract abstract abstract
56 abstract abstract abstract abstract abstract abstract abstract abstract abstract
57 abstract abstract abstract abstract abstract abstract abstract abstract abstract
58 abstract abstract abstract abstract abstract abstract abstract abstract abstract
59 abstract abstract abstract abstract abstract abstract abstract abstract abstract
60 abstract abstract abstract abstract abstract abstract abstract abstract abstract
61 abstract abstract abstract abstract abstract abstract abstract abstract abstract.

Contents

63	Acknowledgements	iii
64	Abstract	iv
65	Contents	v
66	Preface	vii
67	1 Introduction	1
68	2 Theoretical Background	2
69	2.1 The Standard Model	2
70	2.1.1 The Standard Model Structure	2
71	2.1.2 Electroweak Symmetry Breaking and the Higgs	3
72	2.1.3 The Standard Model Parameters	4
73	2.2 Collider Physics and the Higgs	4
74	2.2.1 Higgs Discovery at the LHC	7
75	2.2.2 $t\bar{t}H$ Production	8
76	2.3 Conclusion	10
77	3 The Large Hadron Collider and the ATLAS Experiment	11
78	3.1 The Large Hadron Collider	11
79	3.1.1 The Accelerator Complex	11
80	3.1.2 Beam Parameters and Collisions	12
81	4 Electrons	14

82	4.1	Electrons at Hadron Colliders	14
83	4.2	Reconstruction of Electron at ATLAS	14
84	4.3	Identification of Electrons at ATLAS	14
85	4.3.1	Pile-up	14
86	4.3.2	Trigger vs. Offline	14
87	4.3.3	2011 Menu	14
88	4.3.4	2012 Menu	14
89	4.3.5	Electron Likelihood	14
90	4.4	Measurement of Electron Efficiency at ATLAS	14
91	4.4.1	Techniques	14
92	4.4.2	Issues	14
93	5	Search for the TTH Decay in the Multilepton Channel	15
94	5.1	Signal Characteristics	15
95	5.2	Background Overview	16
96	5.3	Analysis Strategy	17
97	6	Dataset and Simulation	18
98	6.1	Data	18
99	6.1.1	The 2012 Dataset	18
100	6.2	Simulation	19
101	6.2.1	Signal Simulation	20
102	6.2.2	Background Simulation	20
103	6.3	Analysis Overview and Signal Characteristics	21
104	7	Conclusions	22
105	7.1	Higgs Results in Review	22
106	7.2	Prospects for Future	22
107	Bibliography		23

Preface

109 This is the preface. Blah blah blah blah blah blah. Blah blah blah blah blah blah. Blah
110 blah blah blah blah blah blah. Blah blah blah blah blah blah. Blah blah blah blah blah blah
111 blah. Blah blah blah blah blah blah. Blah blah blah blah blah blah. Blah blah blah blah
112 blah blah blah. Blah blah blah blah blah blah. Blah blah blah blah blah blah. Blah blah
113 blah blah blah blah. Blah blah blah blah blah blah. Blah blah blah blah blah blah.
114 Blah blah blah blah blah. Blah blah blah blah blah.

115 Blah blah blah blah blah blah. Blah blah blah blah blah blah. Blah blah blah blah blah
116 blah. Blah blah blah blah blah blah. Blah blah blah blah blah blah. Blah blah blah
117 blah blah blah. Blah blah blah blah blah blah. Blah blah blah blah blah blah. Blah
118 blah blah blah blah blah. Blah blah blah blah blah blah. Blah blah blah blah blah
119 blah. Blah blah blah blah blah blah. Blah blah blah blah blah blah. Blah blah blah
120 blah blah.

Chris Lester
CERN, Fall 2014

¹²²

CHAPTER 1

¹²³

Introduction

¹²⁴ Here is a citation [?].

125

CHAPTER 2

126

Theoretical Background

127 The Standard Model of particle physics (SM) is an extraordinarily successful description of the funda-
128 mental constituents of matter and their interactions. Experiments over the past 50 years have verified
129 the extremely precise prediction of the SM. This success has culminated most recently in the discovery
130 of the Higgs Boson. This chapter provides a brief introduction to the structure of the SM and how
131 scientists are able to test it using hadron collider but focuses primarily on the physics of the Higgs
132 boson and its decays to top quarks. Particular attention is given to the importance of a measurement
133 of the rate at which Higgs Bosons are produced in association of top quarks in the context of testing
134 the predictions the SM.

135 **2.1 The Standard Model**

136 **2.1.1 The Standard Model Structure**

137 The Standard Model (SM) [1, 2, 3, 4] is an example of a quantum field theory that describes the
138 interactions of all of the known fundamental particles. Particles are understood to be excitations of
139 the more fundamental object of the theory, the field. The dynamics and interactions of the fields are
140 derived from the Standard Model Lagrangian, which is constructed to be symmetric under transfor-
141 mations of the group $SU(3) \times SU(2) \times U(1)$. $SU(3)$ is the group for the color, $SU(2)$ is the group for
142 weak iso spin, and $U(1)$ is the group for weak hyper-charge.

143 Gauging the symmetries demands the introduction of 8 massless gluons, or the boson (full integer
144 spin) carriers of the strong force [5] from the generators $SU(3)$ symmetry, and the 4 massless bosons,
145 carriers for the weak and electromagnetic forces from the 3 generators of the $SU(2)$ and 1 generator
146 of the $U(1)$ group. The weak and the electromagnetic forces are considered part of a larger single

¹⁴⁷ unified electroweak group $SU(2) \times U(1)$ and the associated generators mix.

¹⁴⁸ The gauge symmetry allows the theory to be re-normalizable [6], meaning that unwanted infinities
¹⁴⁹ can be absorbed into observables from theory in a way that allows the theory to be able to predict
¹⁵⁰ physics at multiple energy scales. Singlets of the $SU(3)$ group are fermions (half-integer spin particles)
¹⁵¹ called leptons and do not interact with the strong, whereas doublets of the $SU(3)$ group are called
¹⁵² quarks and do interact with the strong force. The SM is a chiral theory: the weak force violates parity,
¹⁵³ as it only couples to left-chiral particles or right-chiral antiparticles. This means that right-chiral and
¹⁵⁴ left-chiral fermions arise from different fields, which are different representations of the weak isospin
¹⁵⁵ group.

¹⁵⁶ The discovery of particles and new interactions in various experiments is intertwined with the
¹⁵⁷ development of the theory that spans many decades and is not discussed in detail here.

¹⁵⁸ So far, 3 separate generations of both quarks and leptons have been discovered, differing only by
¹⁵⁹ mass. The gluon and the 4 electroweak bosons have also been discovered (W^+ , W^- , Z^0 , and γ) ¹. The
¹⁶⁰ reason for this 3-fold replication is not known.

¹⁶¹ 2.1.2 Electroweak Symmetry Breaking and the Higgs

¹⁶² Despite the simple structure of theory, the discovery of massive fundamental particles creates two sets
¹⁶³ of problems both related to $SU(2) \times U(1)$. First, the force-carrying bosons must enter the theory
¹⁶⁴ without mass or the symmetries will be explicitly broken in the Lagrangian. Second, adding fermion
¹⁶⁵ masses to theory in an ad-hoc way allows the right-chiral and left-chiral fermions to mix. Since they
¹⁶⁶ possess different quantum numbers, as different representations of the weak-isospin group, this too
¹⁶⁷ breaks gauge invariance.

¹⁶⁸ To solve these problems, spontaneous electro-weak symmetry breaking (EWSB) is introduced via
¹⁶⁹ the Brout-Englert-Higgs mechanism [7, 8, 9]. A massive scalar field in an electro-weak doublet is
¹⁷⁰ added to the theory with 4 new degrees of freedom and a potential which includes a quartic self-
¹⁷¹ interaction term. Each fermion field interacts with the scalar field via a different Yukawa coupling,
¹⁷² which unites the left and right chiral fields of a single particle type. This field explicitly preserves all
¹⁷³ of the symmetries, but the minimum of the potential does not occur when the expectation of the field
¹⁷⁴ is zero. The field eventually falls to a state, where it acquires a vacuum-expectation value. However,
¹⁷⁵ a non-zero field must therefore point in a particular direction of weak-isospin space, breaking the
¹⁷⁶ symmetry.

¹The actual particles observed to be produced and propagate may be linear combinations of the underlying generators (for the bosons) or gauge representations (for the fermions).

177 The consequences of this spontaneous symmetry breaking are tremendous. First, the universe
 178 is filled with a field with a non-zero expectation value. The theory can be expanded around this
 179 new value and 3 of the degrees of freedom can be interpreted as the longitudinal polarizations of
 180 the W^+ , W^- , and Z^0 , while the 4th remains a scalar field, called the Higgs field with an associated
 181 particle called the Higgs particle or "Higgs" The weak bosons acquire a mass via their longitudinal
 182 polarizations and the Yukawa couplings of the scalar field to the fermions now behave like a mass
 183 term at the this new minimum.

184 **2.1.3 The Standard Model Parameters**

185 Although the SM structure is set by specifying the gauge groups, the EWSB mechanism, and ac-
 186 knowledging the 3-fold replication of the fermions, confronting the SM with experiment requires the
 187 measurement of 17^2 free parameters, which are unconstrained from the theory. These free parameters
 188 include the fermion masses (from the Yukawa coupling), the force coupling constants, the angles and
 189 phase of the mixing between quarks, and constants from the Higgs and electroweak sector³.

190 Experiments have provided a number of measurements of the parameters of the SM[10]. Prior
 191 to the discovery of the Higgs boson (discussed later) the Higgs mass, however, was the only fully
 192 unconstrained parameter, although its value could be inferred via its involvement in loop corrections
 193 on the top mass (M_t) and the W mass (M_W). The GFitter collaboration assembles all relevant
 194 electroweak observable measurements into a statistical model and then allows certain measurements to
 195 float within their uncertainty to allow for a fit among multiple correlated measurements measurements
 196 [11]. Figure 2.1 shows the fitted constraints on 4 key SM parameters (M_H , M_W , M_t , $\sin^2\theta_w$) with
 197 actual measurements overlaid. The addition to the fit of the measured Higgs mass from the ATLAS
 198 and CMS collaborations creates a small tension, as the other observables prefer the mass to be much
 199 lower (~ 80 GeV/ c^2). The tension in the combined electroweak fit (including the Higgs) is not
 200 statistically significant with a p -value of 0.07.

201 **2.2 Collider Physics and the Higgs**

202 To test the theory, physicists accelerate particles to extremely high energies and force them to interact
 203 through collisions. Typically, the particles accelerated are electrons or protons, since they are stable.

²There are additional parameters from neutrino mass terms and mixing but it is unclear how to include these into the Standard Model, since it does not predict right-chiral neutrinos

³ The electroweak sector includes parameters like mass of the W^\pm and Z^0 bosons, the weak mixing angle, $\sin^2\theta_w$, the fermi constant G_F , and Higgs Mass and vacuum expectation value. These parameters however are not wholly independent. As discussed above, it is only necessary theoretically to specify the two parameters relevant to the Higgs potential and the two coupling associated with the gauge groups

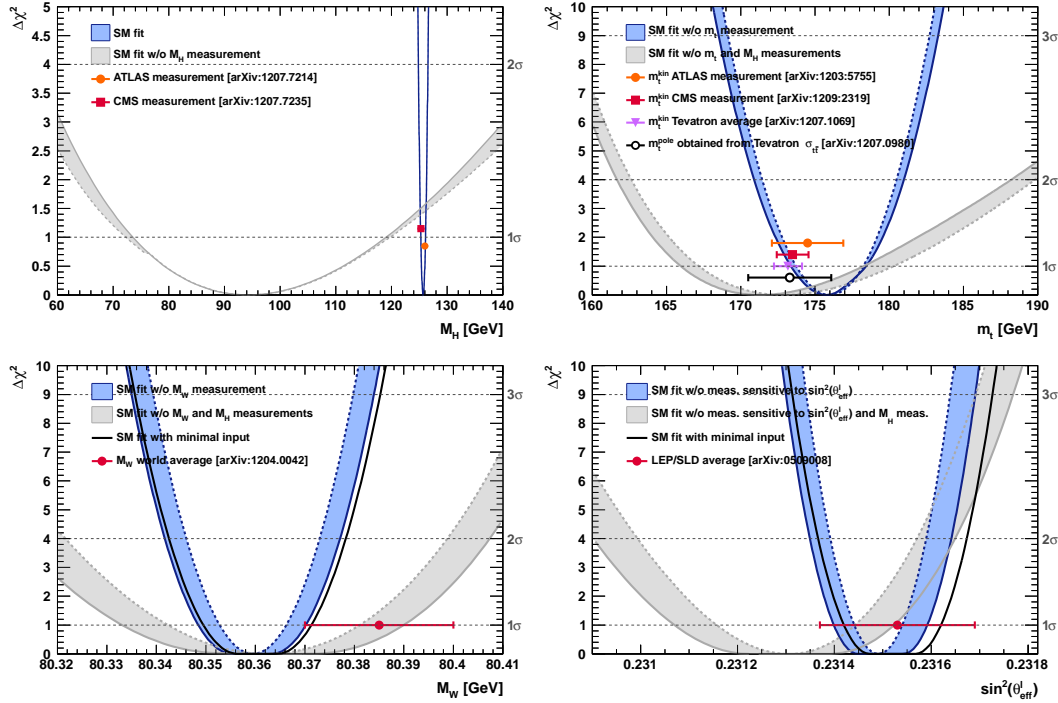


Figure 2.1: χ^2 as a function of the Higgs mass (top left), the top quark mass (top right), the W boson mass (bottom left) and the effective weak mixing angle (bottom right) for the combined SM fit from the GFitter group. The data points placed along $\chi^2 = 1$ represent direct measurements of the respective observable and their $\pm 1\sigma$ uncertainties. The grey (blue) bands show the results when excluding (including) the new M_H measurements from (in) the fits.

204 Electron-positron collider machines have a rich history of discovery and measurement in particle
 205 physics. The advantage of electron accelerators is that the colliding element is itself a fundamental
 206 particle. However, due synchrotron radiation, curvature of the beam line becomes problematic for
 207 high energy beams. Hadron colliders, specifically, proton-proton and proton-anti-proton colliders can
 208 be accelerated in rings without large losses due to synchrotron radiation, but the actual colliding
 209 objects at high energies are the constituent quarks and gluons. This complicates analysis because the
 210 initial state of the system is not discernible on a per-collision basis and momentum of hard scatter
 211 system is unknown along the beam direction.

212 Collider physics rely on form-factor descriptions of the colliding hadrons that describe the fraction
 213 of momentum carried by the hadrons constituent 'partons'. These are called parton-distribution
 214 functions, seen in Figure 2.2, and are factorized and integrated through the theoretical calculations
 215 of various collision processes [12].

216 At the Large Hadron Collider or LHC (discussed in detail in Chapter 3 a proton-proton colluder,

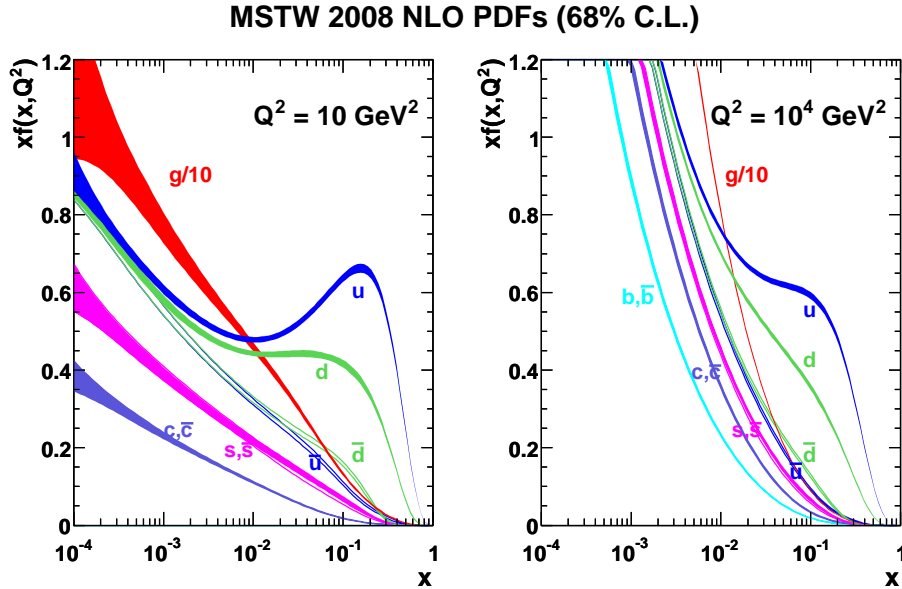


Figure 2.2: Proton Parton Distribution Functions (PDFs) form the MSTW Collaboration at $Q^2 = 10 \text{ GeV}^2$ and $Q^2 = 10^4 \text{ GeV}^2$

the types of initial states are quark-quark, quark-gluon, and gluon-gluon. Gluon collisions dominate overall, due to the large number of gluons inside the proton, though the relative importance of different initial states changes with the energy scale of the collision and the type of final state sought after.

A prime motivation for the construction of the Large Hadron Collider was the discovery or exclusion of the Higgs boson[13]. LEP and the Tevatron excluded large swaths of possible Higgs boson masses, especially below $114 \text{ GeV}/c^2$ and the unitarity of certain diagrams including the $WWWW$ vertex required the mass to be below about 1 TeV, a range that was achievable at the LHC with high luminosity running [10].

Despite the ubiquity of Higgs couplings, Higgs boson production at the LHC is a low rate process. Because it couples to fermions proportional to mass and because the colliding particles must be stable and therefore light, production of the Higgs must occur through virtual states.

The Higgs boson can be produced through collision at the LHC via 4 mechanisms: gluon-fusion (ggF), vector-boson fusion (VBF), Higgsstrahlung (VH), and production in association with top quarks ($t\bar{t}H$). The diagrams are shown in Figure 2.3 and the production cross-sections as a function of Higgs mass for the 8 TeV LHC proton-proton running are shown in Figure 2.4 [14]. The largest production cross-section is via the gluon fusion channel at 20 pb, which proceeds through a fermion loop that is dominated by the top quark, because of its large Yukawa coupling to the Higgs.

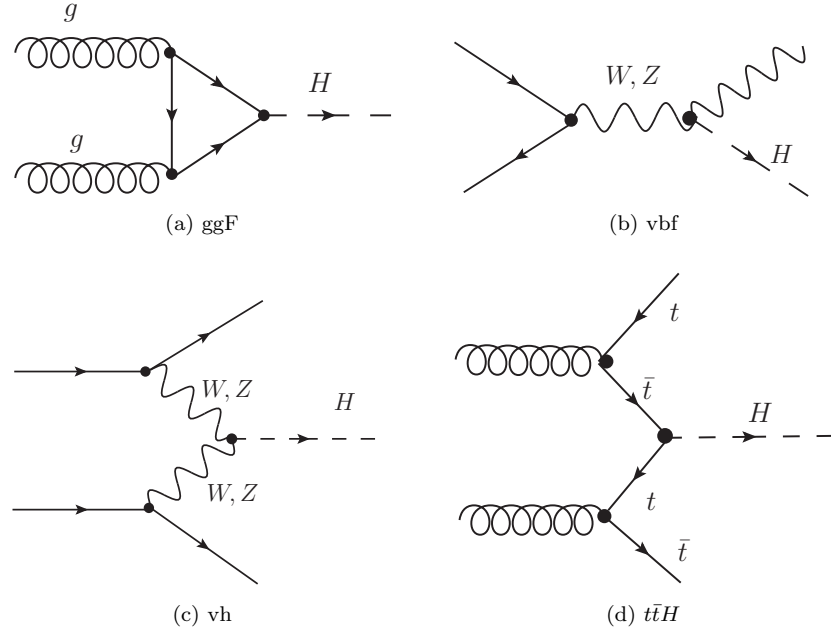


Figure 2.3: Dominant Higgs production modes at the LHC

Because the Higgs' couples to every massive particle, it has a rich set of decays also seen in Figure 2.4, especially for $m_H = 125$. Studies of Higgs properties at hadron colliders offers many tests of the Standard Model and ample room for searches for new physics. These tests specifically can verify the link between Yukawa coupling and the particles mass and further constrain details of EWSB by examining Higgs coupling to the weak bosons.

2.2.1 Higgs Discovery at the LHC

In 2012 both ATLAS and CMS announced the discovery of a new boson consistent with the Higgs by examining the results of Higgs searches in a number of decay channels ($H \rightarrow W^+W^-$, $H \rightarrow Z^0Z^0$, and $H \rightarrow \gamma\gamma$) in the 2011 dataset at $\sqrt{s} = 7$ TeV and part of the 2012 dataset at $\sqrt{s} = 8$ TeV. By 2013 and 2014, both experiments have updated and/or finalized their results for the full 2011 and 2012 datasets [15, 16]. I will focus on the ATLAS results in the following. The ATLAS measurements constrain both the Higgs mass[17] and spin[18], as well as provide constraints to the Higgs couplings to different particles.

Figure 2.5 show the results of the searches in all of the measurement channels as well as constraints on the SM Higgs coupling parameters in an example fit, where the couplings to the top-quark, bottom-

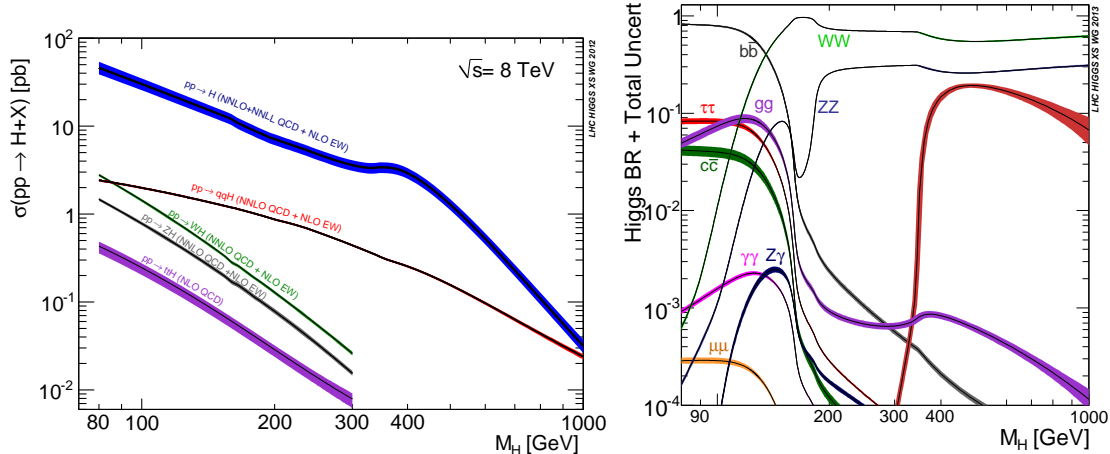


Figure 2.4: 8 TeV LHC Higgs production cross-sections (left) and decay branching fractions

quark, W,Z, and τ are allowed to fluctuate independently. These rely on measurements binned in different production and decay channels. They are dominated by higher statistics results in the gluon-fusion production modes, but measurements in the VH and VBF modes are close to SM sensitivity.

The combined results show basic agreement with the SM with much room for improvement with the addition of new production and decay modes and higher statistics. The coupling constraints are particularly strong for the W and Z, which are the most sensitive decay channels, and top quark due to the dominance of the top Yukawa in the ggF loop.

2.2.2 $t\bar{t}H$ Production

Notably absent thus far in the SM are searches for the Higgs in the $t\bar{t}H$ production channel, due to the lack of statistics. Searches are underway and initial results are close to SM sensitivity for ATLAS and CMS. More will be discussed about particular searches later. $t\bar{t}H$ production depends on the top Yukawa coupling at tree level. Comparison of the gluon-fusion and the $t\bar{t}H$ modes would allow for disentangling the effects of new particles in the gluon-fusion loop[19]. For instance, generic models would allow for the introduction of new colored particles into the loop. The simplest of these models would be the addition of a new generation of quarks. Fourth generation quarks, which obtain mass from a Higgs Yukawa coupling are already largely excluded due to their enormous effects on the Higgs production cross-section[20]. Other exotic scenarios allow for new colored particles in the gluon-fusion loop, which are not entirely constrained by present measurements[21, 22, 23]. These include, for instance, Supersymmetric models involving the stop quark.

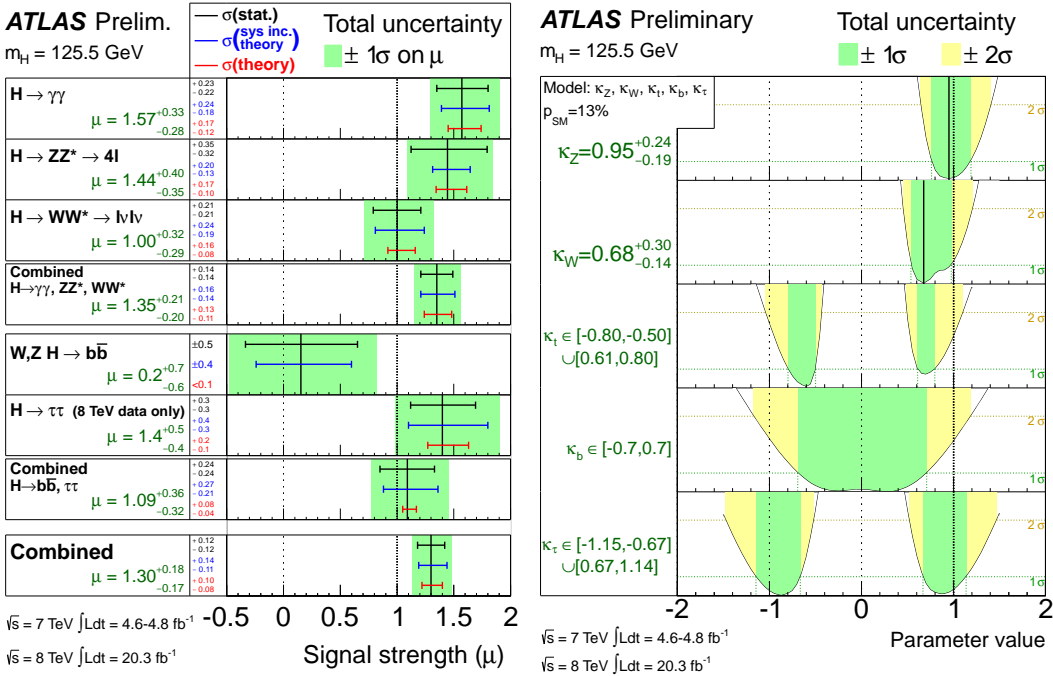


Figure 2.5: ATLAS Higgs combination results for all SM measurement channels as ratios of the measured to SM production cross-sections (left) and extracted Higgs coupling constraint scale-factors for a combined fit to the measurement channels, where the W, Z , top-quark, b -quark, and τ couplings are allowed to float. The p-value of this particular model is 0.13 and in agreement with SM expectations

268 Aside from the loop effects, measurement of the $t\bar{t}H$ production cross-section would provide a
 269 precise measurement of the top Yukawa coupling. When compared with the measured top quark mass,
 270 this tests the Higgs mass generation properties for up-type quarks. Despite similar uncertainties on
 271 the overall production cross-sections for $t\bar{t}H$ and the gluon-fusion modes, both of which depend on the
 272 top Yukawa, most of these uncertainties would cancel for $t\bar{t}H$ if normalized to the topologically similar
 273 $t\bar{t}Z$. Finally, the uniqueness of the experimental signature means that searches for $t\bar{t}$ signatures can
 274 be performed for a variety of Higgs decays ($\gamma\gamma, b\bar{b}, WW, ZZ$, and $\tau\bar{\tau}$ with roughly similar degrees of
 275 sensitivity (within a factor of 10)[19].

276 It is important to note the importance of the top Yukawa coupling to the overall structure of the
 277 SM, due to its enormous size compared to other couplings. The top Yukawa is for instance 350000x as
 278 large as the electron Yukawa coupling. Because of this the top Yukawa coupling, along with the Higgs
 279 mass, is one of the most important pieces of the renormalization group equations (RGE) responsible
 280 for the running of the parameter that determines the Higgs self-coupling λ . If this parameter runs
 281 negative, then the potential responsible for the entire mechanism of EWSB no longer has a minimum
 282 and becomes unbounded, resulting in instability in the universe [24]. Metastability occurs when the

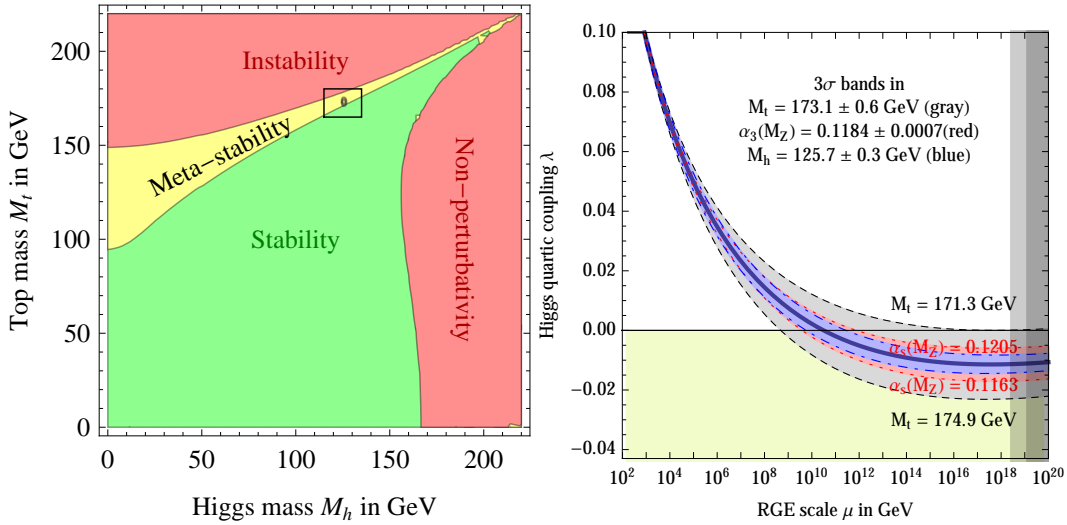


Figure 2.6: RGE for the running of the SM parameter, λ for the Higgs self-coupling term with present values and uncertainty bands for M_H and M_t (left). The two-dimensional plot colored (right) shows regions for which the SM is stable, unstable and metastable based on this RGE

shape of the potential allows for a false local minimum. Figure 2.6 shows the running of this parameter, the regions for which the universe is stable, unstable and metastable. Current measurements suggest that universe lies in a metastable island⁴.

2.3 Conclusion

The Standard Model, despite its success in providing a unified description of fundamental particles and interactions into single theory, has its flaws. These have been discussed in depth elsewhere, but include issues like the description of massive neutrinos, the failure to include gravity, and the unnaturalness of large quantum corrections to Higgs parameters. For these reasons, it seems the SM might be a lower energy approximation to a more fundamental theory. The discovery of the Higgs boson at the LHC provided a stunning verification of one of the fundamental aspects of the theory but at the same time offers new area to search for glimpses of something grander. The production of samples of Higgs bosons allows for a rich array of new tests of the Standard Model, which is now finally over-constrained by experiment. Searches for the $t\bar{t}H$ production, one category of which is the topic of this thesis, provide tree-level access to a central parameter of the theory, the top Yukawa coupling, as well as access a variety of Higgs decays, which will eventually provide a rigorous new test of the SM.

⁴The RGE assumed that there is no new physics at all energy scales

299

CHAPTER 3

300

The Large Hadron Collider and the ATLAS Experiment

301

3.1 The Large Hadron Collider

302 Production of a sufficient number of high energy collisions to adequately explore particle physics at
303 the electro-weak scale required the development of one of the most complex machines ever built, the
304 Large Hadron Collider or LHC.

305 The LHC is the world's highest energy particle accelerator and is located 100m underneath the
306 Franco-Swiss border at the European Organization for Nuclear Research (CERN) in a 26.7 km tunnel.

307 The technology involved in the development of the LHC and very briefly touched upon in this
308 chapter is an enormous achievement in its own right and is documented in detail here [25, 26, 27].

309 The LHC is a circular machine capable of accelerating beams of protons and colliding them at
310 center of mass energies up to $\sqrt{s} = 14\text{TeV}$ at 4 collision sites around the ring, where 4 experiments are
311 housed (ATLAS[28], CMS[?], LHCb[29], and ALICE[?]). Figure 3.1 is a diagram of the layout of the
312 LHC and its experiments[30]. The LHC also operates in modes with beams of heavy ions. The LHC
313 is composed of thousands of super-conducting Niobium-Titanium magnets, cooled to 2.7° C with
314 liquid Helium, which steer and focus the particle beams, and a superconducting resonant-frequency
315 (RF) cavity, which boosts the beam to higher energies.
316

3.1.1 The Accelerator Complex

317 The accelerator complex is a progressive series of machines with the LHC as the final stage. Protons are
318 obtained from hydrogen atoms and are accelerated to 50 MeV using the Linac2, before being injected
319 into the Proton-Synchrotron Booster (PSB). In the PSB the protons are accelerated to energies of 1.4
320

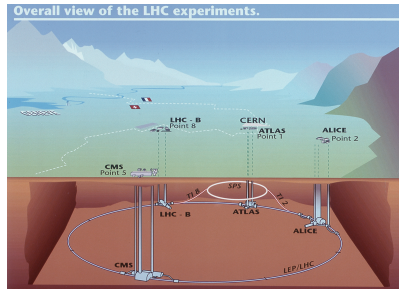


Figure 3.1: Diagram of the Large Hadron collider and location of the 4 main experiments (ATLAS, CMS, LHCb, and ALICE). Around the ring. The diagram also shows the location of the SPS, the final booster ring the accelerator complex that accelerates the protons to 450 GeV before injection into the LHC.

321 GeV for injection in to the Proton-Synchrotron (PS). The PS accelerates the protons to 25 GeV and
 322 dumps bunches into the Super Proton Synchrotron (SPS), where they are accelerated to 450 GeV
 323 and finally dumped into the LHC.

324 3.1.2 Beam Parameters and Collisions

325 For the physics studied at the ATLAS experiment, the two most important parameters of the collisions
 326 provided by the LHC are the center of mass energy and instantaneous luminosity. High center of mass
 327 energies are necessary for the production of new high mass particles, and because the constituents of
 328 the actual collisions are the partons of the proton, the CME of the collisions must in general be much
 329 higher than the mass of the particles needed to be produced. The

330 The instantaneous luminosity of the collisions, \mathcal{L} , is a measure of the collision rate. The integrated
 331 luminosity over time is a measure of the size of the dataset and when multiplied by the cross-section of a
 332 particular process gives the total number of expected events produced for that process. Instantaneous
 333 luminosity depends on the number of colliding bunches of protons, the intensity of those bunches, the
 334 revolution frequency, and the nomralized transverse spread of the beam in momentum and position
 335 phase space, called the emmitance, and the transverse beam size. The LHC has the option for colliding
 336 beams with 2808 bunches of protons, each with around 10^{11} protons, at a rate of one bunch collision
 337 every 25 ns, or 40 MHz. These correspond to a design luminosity of around $10^{34} \text{ cm}^2 \text{ s}^{-1}$ or 10 nb^{-1}

$_{338} \text{ s}^{-1}$

339

CHAPTER 4

340

Electrons

341 **4.1 Electrons at Hadron Colliders**

342 **4.2 Reconstruction of Electron at ATLAS**

343 **4.3 Identification of Electrons at ATLAS**

344 **4.3.1 Pile-up**

345 **4.3.2 Trigger vs. Offline**

346 **4.3.3 2011 Menu**

347 **4.3.4 2012 Menu**

348 **4.3.5 Electron Likelihood**

349 **4.4 Measurement of Electron Efficiency at ATLAS**

350 **4.4.1 Techniques**

351 **4.4.2 Issues**

CHAPTER 5

Search for the TTH Decay in the Multilepton Channel

355 This chapter provides an overview of the set of analyses searching for the Standard Model (SM)
 356 production of the Higgs boson in association with top quarks in multi-lepton final states with multiple
 357 jets (including b-quark tagged jets). Searches in $t\bar{t}H$ final states with 2 same-charge, 3 and 4 light
 358 leptons (e, μ) are discussed in depth. These final states target specifically Higgs decays to vector
 359 bosons, $H \rightarrow W^\pm W^\pm$ and $H \rightarrow Z^\pm Z^\pm$ and form a complement to searches for $t\bar{t}H$ production in
 360 final states targeting the $H \rightarrow b\bar{b}$ [?], $H \rightarrow \gamma\gamma$ [?], and $H \rightarrow \tau\tau$ decay modes.

361 Based on SM production cross-sections, observation lies just outside the sensitivity of the Run I
 362 dataset, even when combining all searches. The analyses provide an opportunity to constrain for the
 363 first time the $t\bar{t}H$ production mode with limits reasonably close to the actual production rate. As
 364 such the analysis is optimized to overall sensitivity to the $t\bar{t}H$ production rather than individual decay
 365 modes, which would be more useful for constraining Higgs couplings.

366 Detailed description of the event and objection section are provided in Chapter ??, background
 367 modelling in Chapter ??, the effect of systematic errors and the statistical analysis in Chapter ?? and
 368 final results in Chapter ??.

369 **5.1 Signal Characteristics**

370 $t\bar{t}H$ can be observed in a number of different final states related to the Higgs boson and the top
 371 quark decay modes.

372 Three Higgs boson decays are relevant for this analysis: W^+W^- , $\tau^+\tau^-$ and ZZ . The top and
 373 anti-top quarks decay in $W^\pm b$. Each W^\pm boson decays either leptonically ($l=e^\pm, \mu^\pm, \tau^\pm$) with missing

374 energy or hadronically. Table 5.1 provides the fractional contribution of the main Higgs decay modes
375 at the generator level to $t\bar{t}H$ search channels. These numbers will be modified by lepton acceptances.

Table 5.1: Contributions of the main Higgs decay modes to the 3 multilepton $t\bar{t}H$ signatures at generation level.

Signature	$H \rightarrow WW$	$H \rightarrow \tau\tau$	$H \rightarrow ZZ$
Same-sign	100%	–	–
3 leptons	71%	20%	9%
4 leptons	53%	30%	17%

376 All modes are generally dominated by the WW signature, though the 3l and 4l channels possess
377 some contribution from the $\tau\tau$ and ZZ decays.

378 The signal is expected to be characterized by the presence of 2 b-quark jets from the top quark
379 decays, leptons from vector boson and tau decays, a high jet multiplicity, and missing energy. In
380 general, the number of leptons is anti-correlated with the number of jets, since a vector boson can
381 either decay leptonically or hadronically. For $H \rightarrow W^+W^-$, the light quark multiplicity, N_q , and the
382 number of leptons, N_l , follow this relation: $2N_l + N_q + N_b = 10$.

- 383 • In the same-sign channel, the $t\bar{t}H$ final state contains 6 quarks. These events are then charac-
384 terised by a large jet multiplicity.
- 385 • In the 3 lepton channel, the $t\bar{t}H$ final state contains 4 quarks from the hard scatter.
- 386 • In the 4 lepton channel, the $t\bar{t}H$ final state contains a small number of light quarks, 0 ($H \rightarrow$
387 W^+W^- case), 2 or 4 ($H \rightarrow ZZ$ case).

388 5.2 Background Overview

389 Background processes can be sorted into two categories:

- 390 • Events with a non prompt or a fake lepton selected as prompt lepton. These processes cannot
391 lead to a final state compatible with the signal signature without a misreconstructed object. This
392 category includes events with a prompt lepton but with misreconstructed charge and events with
393 jets that "fake" leptons.

394 The main backgrounds of this sort are: $t\bar{t}$ and $Z+jets$. Data-driven techniques are used to
395 control some of these processes. Their importance varies depending on the channel.

- 396 • Events which can lead to the same final state as the signal (irreducible backgrounds). The main
397 background of this category are: $t\bar{t}V$, $W^\pm Z$, and ZZ . They are modeled using the Monte
398 Carlo simulations.

399 **5.3 Analysis Strategy**

400 The analysis search is conducted in 3 channels, based on counting of fully identified leptons: 2 SS
401 leptons, 3 leptons, and 4 leptons. The lepton counting occurs before additional object cuts are made in
402 each individual channel to ensure orthogonality. The division into lepton channels rather than channels
403 targeting specific decay modes allows channels with different sensitivities to be considered separately. We
404 further divide the 2l SS into sub channels based on the number of jets and flavor of the leptons and
405 the 4l channel into subchannels enriched and depleted in OS leptons arising from Z decays.

406 The channels are fed into a Poisson model

CHAPTER 6

Dataset and Simulation

409 6.1 Data

410 6.1.1 The 2012 Dataset

411 The LHC successfully produced datasets for physics studies in 2010, 2011 and 2012. The 2012 proton-
 412 proton dataset was delivered with collisions with a CME of 8 TeV with bunch collisions every 50 ns and
 413 reached a total integrated luminosity of around 20 fb^{-1} [31]. Figure 6.1 shows the accumulation of this
 414 dataset over time. Despite doubling the bunch spacing (thereby halving the bunch collision frequency),
 415 the lumonisty neared the design lumonisty due to unexpected improvements in the transverse beam
 416 profile[32]. This increased the amout of pile-up, or number of collisions per bunch crossing and in
 417 general collision events were busier due to these multiple interactions. Figure 6.2 shows the average
 418 number of interaction per bunch crossing for the 2011 and 2012 datasets. The 2012 dataset shows an
 419 average of 20-25 interactions.

420 The $t\bar{t}H$ analysis uses the entire 2012 ATLAS dataset, collected from April to December. The size
 421 of the dataset corresponds to 20.3 fb^{-1} , after passing data quality requirements, ensuring the proper
 422 operation of the tracking, calorimeter and muon subsystems.

423 The datasets used in the analysis were collected with the primary electron (EF_E24VHL_MEDIUM1
 424 — EF_E60_MEDIUM1) and muon triggers (EF_24I_TIGHT — EF_36_TIGHT). The electron
 425 triggers require a electron with at least 25 GeV of calorimeter energy, passing the medium identification
 426 requirement and loose tracking isolation. Above 60GeV, the isolation requirement is dropped and the
 427 identification is loosened slightly. Similarly, the muon trigger requires a good inner detector track and
 428 matching hits in the muon spectrometer, as well as loose tracking isolation, which also is dropped
 429 about 36 GeVThe data sample must contain either a primary muon or primary electron trigger.

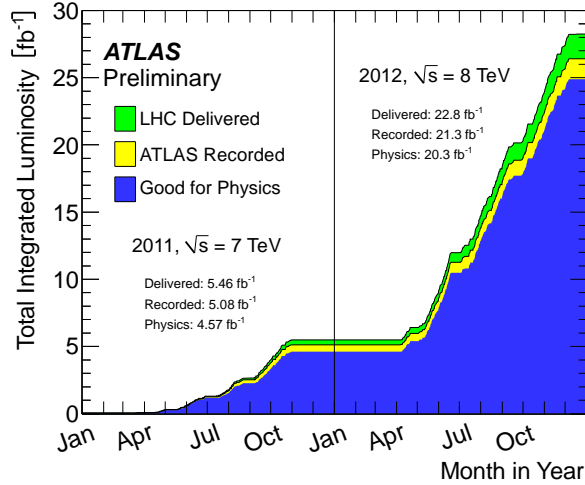


Figure 6.1: Plot showing the accumulation of the integrated luminosity delivered to the ATLAS experiment over 2011 and 2012. The rough size of the usable, physics ready dataset for 2012 is 20 fb^{-1} and is the dataset used for the following analysis.

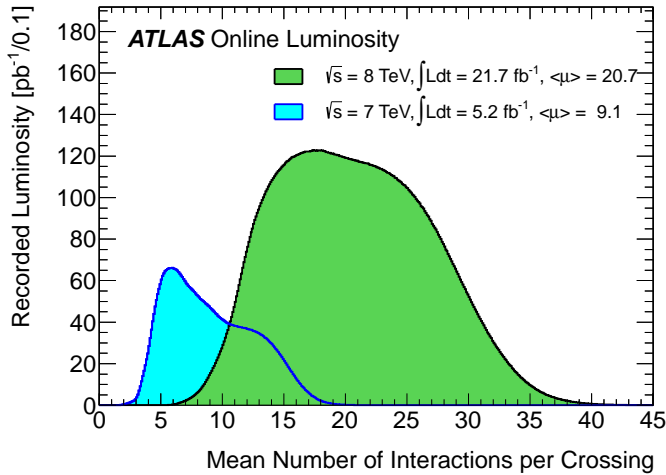


Figure 6.2: The average number of interactions per bunch-crossing for the 2012 and 2011 LHC proton-proton dataset. Most of these interactions are uninteresting but leave energetic signatures in particle detectors called pile-up which interfere with measurements

430 6.2 Simulation

431 Simulation samples based on are used to determine the overall event selection acceptance and efficiency
 432 and for investigations not directly involved in the final result. The simulated samples are created using
 433 parton distribution function (PDF) and model using Monte Carlo (MC) techniques the hard parton
 434 scatter, underlying event activity and parton showering and hadronization. The samples are then

Table 6.1: Monte Carlo samples used for signal description.

Process	Generator	Cross-section [fb]	\mathcal{L} [fb $^{-1}$]	Detector simulation
$t\bar{t}H \rightarrow \text{allhad} + H$	PowHel+Pythia8	59.09	2146.5	Full
$t\bar{t}H \rightarrow \text{ljets} + H$	PowHel+Pythia8	56.63	2238.9	Full
$t\bar{t}H \rightarrow ll + H$	PowHel+Pythia8	13.58	9332.0	Full

435 passed through a full ATLAS detector simulation[33] based on GEANT4 [34]. Small corrections are
 436 then applied to the overall efficiencies to re-scale object identification efficiencies, energy scales, and
 437 the pile-up, discussed in depth later.

438 6.2.1 Signal Simulation

439 The signal Monte Carlo samples are described in Table 6.1. These large samples are generated with
 440 inclusive Higgs boson decays, with branching fractions set to the LHC Higgs Cross Section Working
 441 Group (Yellow Report) recommendation for $m_H = 125$ GeV [?]. The matrix element calculation is
 442 performed at next-to-leading order (NLO); we use $t\bar{t}H$ Les Houches event format files provided by the
 443 authors of the PowHel software [?], decayed and showered with Pythia8[35]. The CT10[36] parton
 444 distribution function is used for matrix element generation. The inclusive cross section (129.3 fb at
 445 $m_H = 125$ GeV) is also obtained from the Yellow Report [?].

446 6.2.2 Background Simulation

447 The background simulations used for this analysis are listed in Table ???. In general, the Alpgen[37],
 448 MadGraph[38], and AcerMC[39] samples use the CTEQ6L1[40] parton distribution function, while
 449 the Powheg[41], Sherpa[42], are generated with the CT10 PDF. The exception is the MadGraph $t\bar{t}t\bar{t}$
 450 sample, which is generated with the MSTW2008 PDF[43]. The highest order calculations available
 451 are used for cross sections.

Table 6.2: Monte Carlo samples used for background description. Unless otherwise specified MadGraph samples use Pythia 6 for showering and Alpgen samples use Herwig+Jimmy.

Process	Generator	Detector simulation
$t\bar{t}W^\pm, t\bar{t}Z$	MadGraph	Full
tZ	MadGraph	AF2

Table 6.2: Monte Carlo samples used for background description. Unless otherwise specified MadGraph samples use Pythia 6 for showering and Alpgen samples use Herwig+Jimmy.

Process	Generator	Detector simulation
$t\bar{t}t\bar{t}$	MadGraph	Full
$t\bar{t}W^\pm W^\pm$	Madgraph+Pythia8	AF2
$t\bar{t}$	Powheg+Pythia6	Full/AF2
single top tchan	AcerMC+Pythia6	Full
single top schan $\rightarrow l$	Powheg+Pythia6	Full
single top $W^\pm t$	Powheg+Pythia6	Full
$W\gamma^*$	MadGraph	Full
$W\gamma+4p$	Alpgen	Full
W^+W^-	Sherpa	Full
$W^\pm Z$	Sherpa	Full
Same-sign WW	Madgraph+Pythia8	AF2
$ZZ \rightarrow$ Powheg+Pythia8,gg2ZZ+Herwig	Full	
$Z\gamma^*$	Sherpa	Full
$Z+jets$	Sherpa	Full
ggF_H(125)	Powheg+Pythia8	Full

452 6.3 Analysis Overview and Signal Characteristics

453 The signal

Table 6.3: Contributions of the main Higgs decay modes to the 5 multilepton $t\bar{t}H$ signatures at generation level.

Signature	$H \rightarrow WW$	$H \rightarrow \tau\tau$	$H \rightarrow ZZ$
Same-sign	100%	—	—
3 leptons	71%	20%	9%
4 leptons	53%	30%	17%

454

CHAPTER 7

455

Conclusions

456 **7.1 Higgs Results in Review**

457 **7.2 Prospects for Future**

Bibliography

- 459 [1] S. L. Glashow, *Partial-symmetries of weak interactions*, Nucl. Phys. **22** (1961) no. 4, 579. [2.1.1](#)
- 460 [2] S. Weinberg, *A Model of Leptons*, Phys. Rev. Lett. **19** (1967) 1264. [2.1.1](#)
- 461 [3] A. Salam and J. C. Ward, *Gauge theory of elementary interactions*, Phys. Rev. **136** (1964)
763–768. [2.1.1](#)
- 462 [4] S. Weinberg, *Non-abelian gauge theories of the strong interactions*, Phys. Rev. Lett. **31** (1973)
494–497. [2.1.1](#)
- 463 [5] D. J. Gross and F. Wilczek, *Ultraviolet behavior of non-abelian gauge theories*, Phys. Rev. Lett.
30 (1973) 1343–1346. [2.1.1](#)
- 464 [6] G. 't Hooft and M. Veltman, *Regularization and renormalization of gauge fields*, Nuclear
Physics B **44** (1972) 189 – 213. [2.1.1](#)
- 465 [7] P. W. Higgs, *Broken symmetries and the masses of gauge bosons*, Phys. Rev. Lett. **13** (1964)
508. [2.1.2](#)
- 466 [8] P. W. Higgs, *Spontaneous symmetry breakdown without massless bosons*, Phys. Rev. **145** (1966)
1156. [2.1.2](#)
- 467 [9] F. Englert and R. Brout, *Broken Symmetry and the Mass of Gauge Vector Mesons*,
Phys. Rev. Lett. **13** (1964) 321–322. [2.1.2](#)
- 468 [10] The ALEPH, CDF, DØ, DELPHI, L3, OPAL, SLD Collaborations, the LEP Electroweak
Working Group, the Tevatron Electroweak Working Group, and the SLD electroweak and
heavy flavour groups, *Precision Electroweak Measurements and Constraints on the Standard
Model*, CERN-PH-EP-2010-095 (2010) , [arXiv:1012.2367 \[hep-ex\]](#). [2.1.3](#), [2.2](#)
- 469 [11] M. Baak, M. Goebel, J. Haller, A. Hoecker, D. Kennedy, R. Kogler, K. Mnig, M. Schott, and
J. Stelzer, *The electroweak fit of the standard model after the discovery of a new boson at the
LHC*, The European Physical Journal C **72** (2012) no. 11, .
<http://dx.doi.org/10.1140/epjc/s10052-012-2205-9>. [2.1.3](#)
- 470 [12] J. C. Collins, D. E. Soper, and G. Sterman, *Factorization for short distance hadron-hadron
scattering*, Nuclear Physics B **261** (1985) 104 – 142. [2.2](#)
- 471 [13] CERN, . CERN, Geneva, 1984. [2.2](#)

- 486 [14] LHC Higgs Cross Section Working Group, S. Dittmaier, C. Mariotti, G. Passarino, and
 487 R. Tanaka (Eds.), *Handbook of LHC Higgs Cross Sections: 2. Differential Distributions*,
 488 CERN-2012-002 (CERN, Geneva, 2012) , [arXiv:1201.3084 \[hep-ph\]](https://arxiv.org/abs/1201.3084). 2.2
- 489 [15] *Updated coupling measurements of the Higgs boson with the ATLAS detector using up to 25*
 490 fb^{-1} *of proton-proton collision data*, Tech. Rep. ATLAS-CONF-2014-009, CERN, Geneva, Mar,
 491 2014. 2.2.1
- 492 [16] CMS Collaboration Collaboration, *Precise determination of the mass of the Higgs boson and*
 493 *studies of the compatibility of its couplings with the standard model*, Tech. Rep.
 494 CMS-PAS-HIG-14-009, CERN, Geneva, 2014. 2.2.1
- 495 [17] ATLAS Collaboration Collaboration, G. Aad et al., *Measurement of the Higgs boson mass from*
 496 *the $H \rightarrow \gamma\gamma$ and $H \rightarrow ZZ^* \rightarrow 4\ell$ channels with the ATLAS detector using 25 fb^{-1} of pp*
 497 *collision data*, [arXiv:1406.3827 \[hep-ex\]](https://arxiv.org/abs/1406.3827). 2.2.1
- 498 [18] *Evidence for the spin-0 nature of the Higgs boson using {ATLAS} data*, Physics Letters B **726**
 499 (2013) no. 13, 120 – 144.
 500 <http://www.sciencedirect.com/science/article/pii/S0370269313006527>. 2.2.1
- 501 [19] S. Dawson, A. Gritsan, H. Logan, J. Qian, C. Tully, et al., *Working Group Report: Higgs*
 502 *Boson*, [arXiv:1310.8361 \[hep-ex\]](https://arxiv.org/abs/1310.8361). 2.2.2
- 503 [20] O. Eberhardt, G. Herbert, H. Lacker, A. Lenz, A. Menzel, et al., *Impact of a Higgs boson at a*
 504 *mass of 126 GeV on the standard model with three and four fermion generations*,
 505 Phys.Rev.Lett. **109** (2012) 241802, [arXiv:1209.1101 \[hep-ph\]](https://arxiv.org/abs/1209.1101). 2.2.2
- 506 [21] M. Carena, S. Gori, N. R. Shah, C. E. Wagner, and L.-T. Wang, *Light Stops, Light Staus and*
 507 *the 125 GeV Higgs*, JHEP **1308** (2013) 087, [arXiv:1303.4414](https://arxiv.org/abs/1303.4414). 2.2.2
- 508 [22] N. Arkani-Hamed, K. Blum, R. T. D’Agnolo, and J. Fan, *2:1 for Naturalness at the LHC?*,
 509 JHEP **1301** (2013) 149, [arXiv:1207.4482 \[hep-ph\]](https://arxiv.org/abs/1207.4482). 2.2.2
- 510 [23] D. Carmi, A. Falkowski, E. Kuflik, and T. Volansky, *Interpreting LHC Higgs Results from*
 511 *Natural New Physics Perspective*, JHEP **1207** (2012) 136, [arXiv:1202.3144 \[hep-ph\]](https://arxiv.org/abs/1202.3144). 2.2.2
- 512 [24] G. Degrassi, S. Di Vita, J. Elias-Miro, J. R. Espinosa, G. F. Giudice, et al., *Higgs mass and*
 513 *vacuum stability in the Standard Model at NNLO*, JHEP **1208** (2012) 098, [arXiv:1205.6497](https://arxiv.org/abs/1205.6497)
 514 [hep-ph]. 2.2.2
- 515 [25] L. Evans and P. Bryant, *LHC Machine*, JINST **3** (2008) no. 08, S08001. 3.1
- 516 [26] T. S. Pettersson and P. Lefevre, *The Large Hadron Collider: conceptual design.*, Tech. Rep.
 517 CERN-AC-95-05 LHC, CERN, Geneva, Oct, 1995. <https://cdsweb.cern.ch/record/291782>.
 518 3.1
- 519 [27] T. Linnecar et al., *Hardware and Initial Beam Commissioning of the LHC RF Systems.*
 520 [oai:cds.cern.ch:1176380](https://cds.cern.ch/record/1176380), Tech. Rep. LHC-PROJECT-Report-1172.
 521 CERN-LHC-PROJECT-Report-1172, CERN, Geneva, Oct, 2008.
 522 <https://cdsweb.cern.ch/record/1176380>. 3.1
- 523 [28] ATLAS Collaboration, *The ATLAS Experiment at the CERN Large Hadron Collider*, JINST **3**
 524 (2008) S08003. 3.1

- 525 [29] The LHCb Collaboration, *The LHCb Detector at the LHC*, *Journal of Instrumentation* **3** (2008)
 526 no. 08, S08005. 3.1
- 527 [30] A. Team, *The four main LHC experiments*, Jun, 1999. 3.1
- 528 [31] ATLAS Collaboration, G. Aad et al., *Improved luminosity determination in pp collisions at $\sqrt{s} = 7 \text{ TeV}$ using the ATLAS detector at the LHC*, *Eur.Phys.J.* **C73** (2013) 2518, arXiv:1302.4393
 529 [hep-ex]. 6.1.1
- 530 [32] CERN, . CERN, Geneva, 2012. 6.1.1
- 532 [33] ATLAS Collaboration Collaboration, G. Aad et al., *The ATLAS Simulation Infrastructure*,
 533 *Eur.Phys.J.* **C70** (2010) 823–874, arXiv:1005.4568 [physics.ins-det]. 6.2
- 534 [34] GEANT4 Collaboration, S. Agostinelli et al., *GEANT4: A Simulation toolkit*,
 535 *Nucl.Instrum.Meth.* **A506** (2003) 250–303. 6.2
- 536 [35] T. Sjostrand, S. Mrenna, and P. Z. Skands, *A Brief Introduction to PYTHIA 8.1*,
 537 *Comput.Phys.Commun.* **178** (2008) 852–867, arXiv:0710.3820 [hep-ph]. 6.2.1
- 538 [36] H.-L. Lai, M. Guzzi, J. Huston, Z. Li, P. M. Nadolsky, et al., *New parton distributions for*
 539 *collider physics*, *Phys.Rev.* **D82** (2010) 074024, arXiv:1007.2241 [hep-ph]. 6.2.1
- 540 [37] M. L. Mangano, M. Moretti, F. Piccinini, R. Pittau, and A. D. Polosa, *ALPGEN, a generator*
 541 *for hard multiparton processes in hadronic collisions*, *JHEP* **0307** (2003) 001,
 542 arXiv:hep-ph/0206293 [hep-ph]. 6.2.2
- 543 [38] F. Maltoni and T. Stelzer, *MadEvent: Automatic event generation with MadGraph*, *JHEP* **0302**
 544 (2003) 027, arXiv:hep-ph/0208156 [hep-ph]. 6.2.2
- 545 [39] B. P. Kersevan and E. Richter-Was, *The Monte Carlo event generator AcerMC versions 2.0 to*
 546 *3.8 with interfaces to PYTHIA 6.4, HERWIG 6.5 and ARIADNE 4.1*, *Comput.Phys.Commun.*
 547 **184** (2013) 919–985, arXiv:hep-ph/0405247 [hep-ph]. 6.2.2
- 548 [40] P. M. Nadolsky, H.-L. Lai, Q.-H. Cao, J. Huston, J. Pumplin, et al., *Implications of CTEQ*
 549 *global analysis for collider observables*, *Phys.Rev.* **D78** (2008) 013004, arXiv:0802.0007 [hep-ph].
 550 6.2.2
- 551 [41] S. Frixione, P. Nason, and C. Oleari, *Matching NLO QCD computations with Parton Shower*
 552 *simulations: the POWHEG method*, *JHEP* **0711** (2007) 070, arXiv:0709.2092 [hep-ph]. 6.2.2
- 553 [42] T. Gleisberg, S. Hoeche, F. Krauss, M. Schonherr, S. Schumann, et al., *Event generation with*
 554 *SHERPA 1.1*, *JHEP* **0902** (2009) 007, arXiv:0811.4622 [hep-ph]. 6.2.2
- 555 [43] A. Martin, W. Stirling, R. Thorne, and G. Watt, *Parton distributions for the LHC*, *Eur.Phys.J.*
 556 **C63** (2009) 189–285, arXiv:0901.0002 [hep-ph]. 6.2.2